

Extract of raphanus raphanistrum peel waste as reducing agent for the synthesis of silver and gold nanoparticles

S. Pirathiba*, B. S. Dayananda

M.S. Ramaiah University of Applied Science, Bangalore - 560054, India

Raphanus raphanistrum peel waste extract is utilized for the biological synthesis of silver nanoparticles (Ag NPs) and gold nanoparticles (Au NPs). UV-Visible spectroscopy, scanning electron microscopy, energy-dispersive X-ray spectroscopy, Fourier transform infrared spectroscopy and X-ray powder diffraction analyses are performed to characterize NPs. Further, the catalytic behavior of prepared NPs is elucidated against methylene blue and congo red as model pollutants in the presence of sodium borohydride as a reducing agent. Au NPs have degradation efficiency of 66% and 61% against methylene blue and congo red which is higher than Ag NPs which shows 28% and 25% respectively.

(Receipt Date: 06/12/2021)

(Received December 8, 2021; Accepted March 14, 2022)

Keywords: Gold nanoparticles, Silver nanoparticles, Radish peel waste, *Raphanus raphanistrum*, Catalytic activity

1. Introduction

Nanoscience and technology deal with the use of nanoparticles (NPs) and has become an emerging area of research that focuses on the advancement in various sectors such as healthcare, waste management, electronics, photonics, etc. that ultimately improves the quality of life to humans. Each NPs has its inherent physical, chemical, mechanical, and electrical properties which tend to alter when particle size is changed. Also, the properties of NPs vary based on the technique used for their synthesis. Synthesis of NPs is often performed through chemical, physical, and biological routes. Chemical and physical techniques are employed to synthesis different nano-dimensional structures that use sophisticated instruments, high energy consumption for heat and pressure build-up, harmful capping and stabilizing reagent, etc. Therefore, these techniques can liberate hazardous moieties into the environment reducing the loudness of its applications but also the term "Green world". Hence, in the present global situation, priority has been given to developing eco-friendly technologies for the synthesis of NPs. Potential natural frameworks in plants and micro-organisms are being utilized for NPs synthesis and are termed green synthesis routes. The first scientist to synthesis s Au NPs and Ag NPs using *Medicago sativa* plants is Gardea –Torresday *et al* [1, 2]. Despite, various routes available for the synthesis of metallic NPs, plant extract-based techniques are proven for their rapid and eco-friendly synthesis route. For synthesizing NPs using plant extract, the extract can be prepared from every part of the plant such as leaf, root, stem, seeds, flowers, barks, and shoots. The bioactive agents acting as reductants present in the extract are proteins, amino acids, sugars, secondary structures, flavones, terpenoids, polyols, ascorbic, tartaric acid, enzymes, etc. The key principle of biosynthesis of metallic NPs is the reduction of metal ions to nano-sized metals.

Plant extract-based NPs synthesis routes are dependent on various factors such as temperature, pH, extract concentration, precursor concentration, reaction time, etc. By controlling these factors, it's possible to develop eco-friendly NPs with controlled shape and size. Through the plant extract route, Au NPs are synthesized from extract developed from lemongrass [3], tamarind [4], etc. and Ag NPs are synthesized from geranium plant extract [5], neem leaves [6, 7], hysterothorus leaves [8], etc. Although plant extract-based NPs synthesis routes have gained higher attention in recent years, it involves the usage of plants that have valuable medicinal and

* Corresponding author: vijayakumarprathiba23@gmail.com
<https://doi.org/10.15251/DJNB.2022.171.335>

therapeutic utilization. To overcome this situation, researchers start to focus on the plant wastes for the synthesis of NPs. It employs a set apart approach of the 3R principle i.e., "Recycle, Reuse & Recovery" [9]. The use of green waste materials is inexpensive and extensively available and has the reducing property that of the plant extract. Many plant wastes are used for the synthesis of NPs such as *Annona squamosa* peel waste, plantain fruit peel waste, sweet orange fruit peel waste, rice husk waste, pomegranate peel waste, grape processing waste, coconut coir waste, etc. Still, numerous green waste materials are available that have got to be explored for NPs synthesis.

In this context, the present research focuses on the synthesis of Ag NPs and Au NPs from radish peel waste. Green synthesized NPs are investigated for their size, shape, crystal phase, and purity employing different characterization techniques. *Raphanus raphanistrum* (radish) belongs to the Brassicaceae family and has a consumable root part. It has been cultivated in every part of the world. Radish peel is rich in polyphenols, isothiocyanate, aldehydes, proteins, and organic acids like oxalic and malic acids [10]. These phytochemicals are liable for the reduction of Ag ions and Au ions leading to the formation of Ag NPs and Au NPs. Further, the catalytic behavior of the prepared NPs is elucidated against methylene blue (MB) and congo red (CR) in the presence of an external reducing agent.

2. Materials and methods

2.1. Preparation of extract

The peel waste is first dried using a hot air oven at 105°C for 1 h placed in a crucible and the dry weight is estimated. For the peel waste extract preparation, 2 g of dried peel is sterilized. After the sterilization process, the peels are chopped into small sizes and collected in a 250 ml glass beaker. Add 100 ml distilled water that is allowed to boil for 30 min. During this process, the water-soluble phytochemicals are dissolved in the distilled water that is decanted through Whatman filter paper. After reaching room temperature, the collected extract is preserved in the refrigerator.

2.2. Preparation of metallic solutions

1 mM of silver nitrate (AgNO_3) used as Ag precursor is prepared by dissolving 0.169 g of AgNO_3 in 1000 ml distilled water. Similarly, 1 mM of hydrogen tetrachloroaurate (HAuCl_4) that is used as Au precursor is prepared by dissolving 0.339 g HAuCl_4 in 1000 ml distilled water.

2.3. Biosynthesis of NPs utilizing radish peel waste as reducing agent

Radish peel waste extract (E) and metal precursor solution (M) are taken in different combinations for synthesizing NPs. 1E+9M, 2E+8M, and 3E+7M are the combinations selected for the preparation of Ag NPs (1E+9Ag, 2E+8Ag, and 3E+7Ag) and Au NPs (1E+9Au, 2E+8Au, and 3E+7Au). The phytochemicals present in the extract act as a reducing agent which converts Ag^+ to Ag^0 and Au^{3+} to Au^0 which are then followed by crystal growth leading to the formation of Ag NPs and Au NPs, respectively. Further, the reaction of the reduction process and formation of NPs is followed by a UV-Vis spectrometer. NPs formation is confirmed visually by their color change where yellowish earthy color is obtained for Ag NPs and pinkish brown color for Au NPs. The prepared Ag NPs and Au NPs are found to be stable for more than 48 h because of the existence of capping agents in radish extracts.

2.4. NPs characterization technique

The colloidal metal NPs solutions are ultra-centrifuged for 15 min at 10,000 rpm. The pellet obtained from the centrifugation process is redispersed in distilled water and the process is repeated thrice to remove excess biological impurities from the sample. The washed pellet is air-dried to obtain NPs powder samples which are used for characterization. A scanning electron microscope (SEM, TE SCANVEGA3) combined with energy-dispersive X-ray spectroscopy (EDX) is employed to analyze NPs shape, size, and purity. Xpert 3 powder X-ray diffraction

(XRD) system is used to determine the crystalline phase of the prepared NPs. Fourier transform infrared (FTIR) spectroscopy (Thermo Scientific) with attenuated total reflection mode is used to elucidate the functional groups originating from biological moiety attached to the surface of the particle.

2.5. Catalytic degradation of dyes

Congo red (CR) and methylene blue (MB) dyes are used as the model pollutants to study the catalytic behavior of Ag NPs and Au NPs in the presence of sodium borohydride (SB, NaBH₄).

The experiments are conducted as per the combinations designated as,

A = 1 ml 10 mM SB + 1.5 ml 1 mM MB dye + 7.5 ml double-distilled water.

B = 1 ml 10 mM SB + 1.5 ml 1 mM CR dye + 7.5 ml double-distilled water.

C = 1 ml 10 mM SB + 1.5 ml 1 mM MB dye + 1 ml E + 6.5 ml double-distilled water.

D = 1 ml 10 mM SB + 1.5 ml 1 mM CR dye + 1 ml E + 6.5 ml double-distilled water.

E = 1 ml 10 mM SB + 1.5 ml 1 mM MB dye + 1 ml E-Ag NPs + 6.5 ml double-distilled water.

F = 1 ml 10 mM SB + 1.5 ml 1 mM CR dye + 1 ml E-Ag NPs + 6.5 ml double-distilled water.

G = 1 ml 10 mM SB + 1.5 ml 1 mM MB dye + 1 ml E-Au NPs + 6.5 ml double-distilled water.

H = 1 ml 10 mM SB + 1.5 ml 1 mM CR dye + 1 ml E-Au NPs + 6.5 ml double-distilled water.

For preparing 10 mM of NaBH₄ solution, 0.038 g of NaBH₄ is dissolved in 100 ml distilled water. For preparing 1 mM of dye solution, 0.032 g of methylene blue and 0.07 g of congo red are mixed with 100 ml distilled water separately. Prepared dye and NaBH₄ solutions are stored in a brown, amber bottle and kept in dark.

The dye degradation % is calculated using the equation provided below [11] where A_0 is the initial absorption and A_t is the absorption at time t .

$$\text{Dye degradation \%} = \frac{A_0 - A_t}{A_t} \times 100$$

3. Results and discussion

3.1. UV-visible spectroscopic analysis

The UV-visible spectral outcomes for Ag NPs fabricated employing radish peel extract as reducing agents are presented in Table 1. When radish extract is added to the Ag precursor solution in the combinations 2E+8Ag and 3E+7Ag, the color of the solution changes after 24 h owing to the surface plasmon resonance (SPR) characteristics of Ag NPs present in the reaction mixture. Also, it is found that the increase in extract concentration increases the absorbance (Abs) of Ag NPs at λ_{max} within the range 400-420 nm. After 48 h, the combination 1E+9Ag also showed λ_{max} around 420 nm due to the nucleation and crystal growth of Ag NPs.

Table 1. UV visible spectral analysis reports for Ag NPs and Au NPs.

Reaction Duration	1E+9Ag		2E+8Ag		3E+7Ag		1E+9Au		2E+8Au		3E+7Au	
	λ_{max} (nm)	Abs (a.u.)										
0 h	-	-	-	-	-	-	-	-	-	-	-	-
2 h	-	-	-	-	-	-	-	-	-	-	-	-
4 h	-	-	-	-	-	-	-	-	-	-	534	0.162
6 h	-	-	-	-	-	-	-	-	-	-	532	0.262
24 h	-	-	401	0.537	420	0.617	545	0.170	534	0.472	536	1.381
48 h	420	0.152	420	0.609	420	1.043	-	-	-	-	-	-

The UV-visible spectral analysis reports of Au NPs fabricated utilizing different combinations of radish peel extract are provided in Table 1. When radish extract is added to Au precursor solution, only 3E+7Au combination showed color change after 4 h of reaction time. The other combinations like 1E+9Au and 2E+8Au show Abs for Au NPs only after 24 h of reaction time. This fact validates that the higher percentage of extract leads to the rapid formation of Au NPs. The combination 3E+7Au shows maximum Abs of 1.38 a.u. at λ_{max} 536 nm after 24 h. Unlike Ag Nps, after 48 h of reaction, the Au NPs are destabilized and result in precipitation due to continuous crystal growth through the Ostwald ripening process. This is due to the fact that the biomolecules are inefficient to act as a capping agent for Au NPs and therefore, the Ostwald ripening process cannot be restricted leading to the continuous growth of the crystal. As the crystal grows in size, they are easily aggregated and precipitated due to the improvement in the mass of the particles. Hence, no peak is seen for Au NPs suspension after 48 h of reaction period. Therefore, for uniform experimental studies, NPs prepared after 24 h are taken for experimental studies.

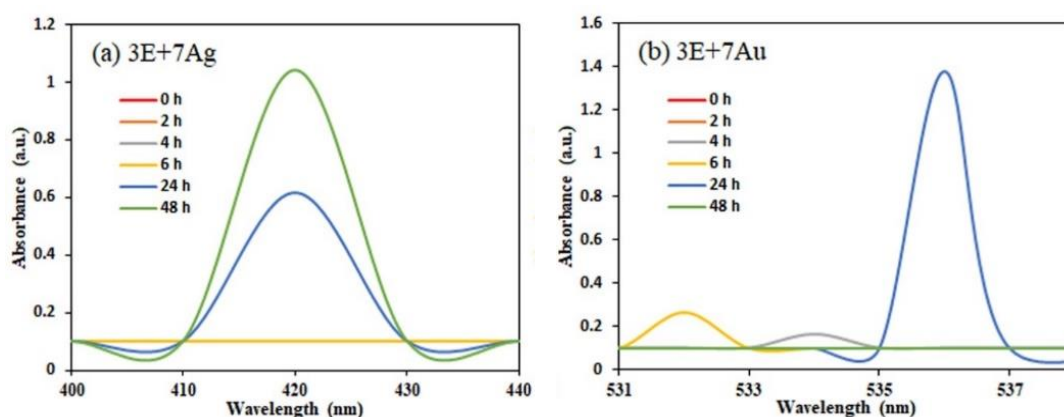


Fig. 1. UV-visible spectra of (a) Ag NPs and (b) Au NPs prepared with radish peel extract using 3E+7M combination.

Fig. 1a shows the UV-Visible spectra of Ag NPs prepared using the combination 3E+7Ag followed from 0 to 48 h. From the UV-Visible spectra, the Ag NPs are formed after 24 h confirmed with the emergence of Abs peak at 420 nm [12]. Further, it is reported that the λ_{max} of Ag NPs is obtained at 430 nm while using red radish extract as a reducing agent [13]. However, the present study shows a blue shift in the λ_{max} value supporting the efficacy of biomolecules acting as a capping agent from the radish peel extract that restricts the growth of crystal and thus, keeping the particle size under control. Moreover, the peak intensity tends to increase as the reaction time increases from 24 h to 48 h.

Fig. 1b shows the UV-Visible spectra of Au NPs prepared in the combination 3E+7Au followed from 0 to 48 h. From the spectra, it is confirmed that the Au NPs are formed or Au ions are reduced by the phytochemicals from radish peels extract after 24 h of reaction time. The emergence of a peak at 536 nm substantiates the formation of Au NPs. However, after 48 h the peak disappears owing to the aggregation and precipitation of Au NPs.

3.2. Morphological and elemental analysis of Ag NPs and Au NPs by SEM with EDX

To differentiate the NPs, the highlight and background of the SEM images are provided with different colors. The SEM images are recorded with 68 k \times magnification using secondary electron (SE) mode. From Fig. 2a, it is confirmed that the Ag NPs are spherical in shape with sizes ranging from 35 nm to 55 nm. The Ag NPs are found agglomerated due to the presence of biological moieties that held the NPs together while drying process. Fig. 2b shows the SEM image of Au NPs that also have spherical-shaped structures with homogeneous size distribution in the

range 40 nm to 50 nm. Here also, the presence of biological components induces aggregation while the drying process.

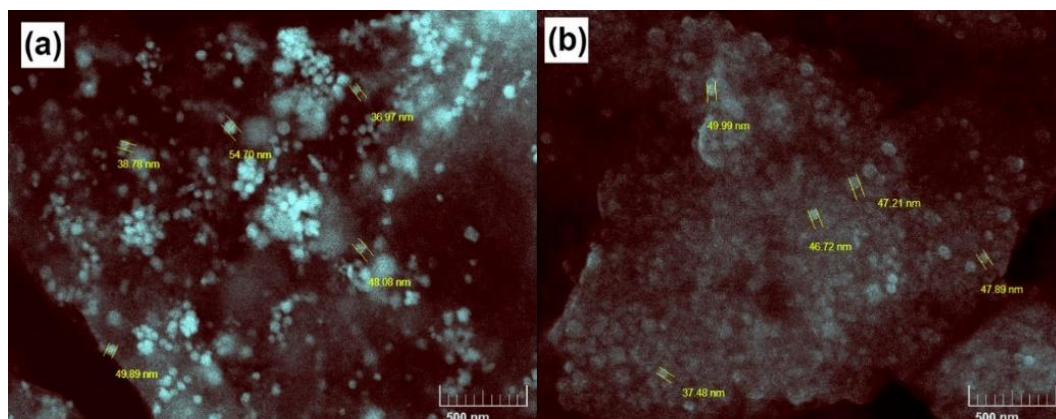


Fig. 2. SEM images of (a) Ag NPs and (b) Au NPs synthesized using radish peel extract.

Further, the elemental composition of Ag NPs and Au NPs is validated through EDX analysis shown in Fig. 3a&b, respectively. The EDX spectra display a strong peak for both Ag and Au with a wt. % of 53.03% and 40.58%, respectively. Along with Ag and Au moieties, C and O are also found to exist in the prepared NPs originated from the phytochemicals attached to the Ag NPs and Au NPs. Hence, it is validated that the Ag NPs and Au NPs are synthesized without any external impurities.

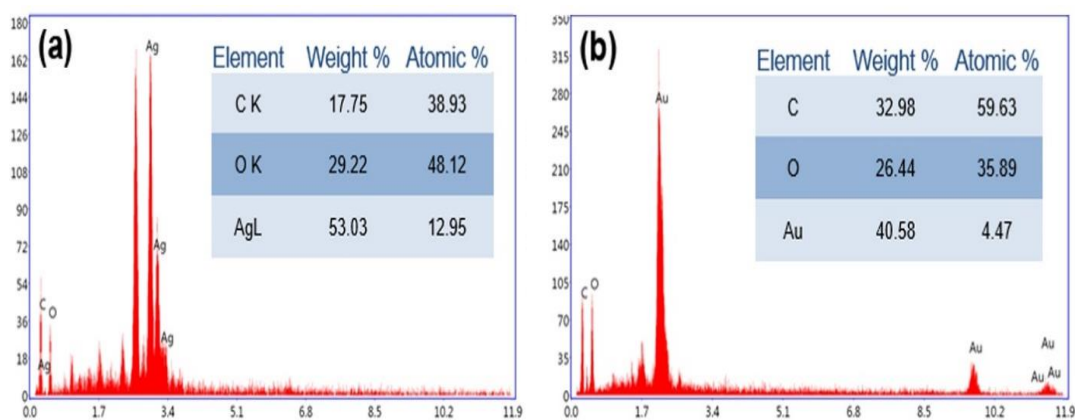


Fig. 3. EDAX spectra of (a) Ag NPs and (b) Au NPs biosynthesized using radish peel extract

3.3. XRD pattern of silver and gold NPs

From the XRD pattern, the crystalline structure of the prepared NPs can be elucidated. In this regard, the XRD patterns of Ag NPs and Au NPs are recorded and presented as Fig. 4a&b, respectively. Fig. 4a displays two diffraction peaks at $2\theta = 38.117^\circ$ and 44.525° originated from the face-centered cubic crystal of Ag NPs corresponding to the miller indices (111) and (200) which are in accordance with JCPDS No. 04-0783 [14]. Along with the diffraction peaks of Ag NPs, two major diffraction peaks are seen (Fig. 4a, represented by *) at $2\theta = 32.225^\circ$ and 46.385° which confirms the presence of biological entities along with Ag NPs [14]. Using the Debye-Scherrer equation shown below [15], the crystallite size of Ag NPs is calculated as 17 nm. From this result, it is clear that the Ag NPs is composed of multiple grains.

$$\text{Crystallite size, } D = \frac{0.9 \times \lambda}{\beta \times \cos\theta}$$

where λ is the wavelength of the X-ray used, β is the full width at half maximum, and θ is derived from diffraction angle (2θ). Fig. 4b shows a single diffraction peak at $2\theta = 38.195^\circ$ originated from the face-centered cubic crystal of Au NPs attributed to the miller index (111) (JCPDS No. 04-0784) [16]. Similar to the XRD pattern of Ag NPs, the diffraction pattern of Ag NPs also displays other diffraction peaks (Fig. 4b, represented by *) which are ascribed to the biological moieties present in the samples. Further, the crystallite size is elucidated from the Debye-Scherrer equation as 14 nm. Like Ag NPs, Au NPs also comprised multiple grains.

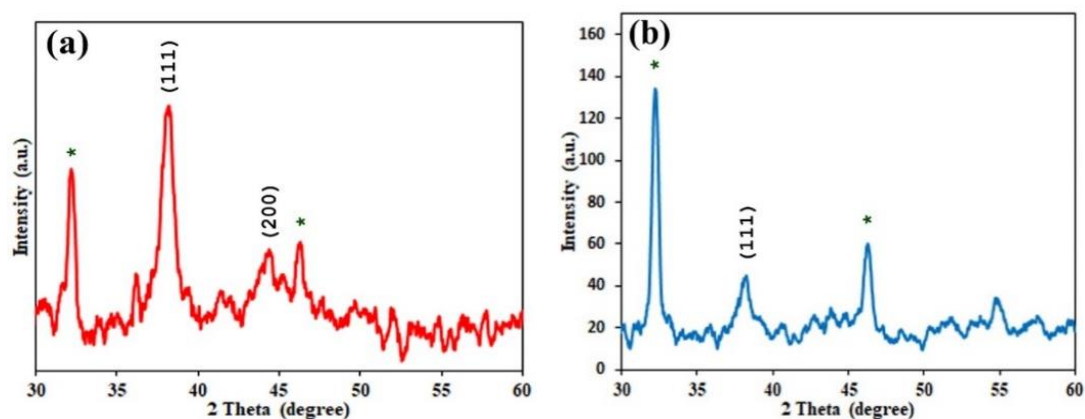


Fig. 4. XRD pattern of (a) Ag NPs and (b) Au NPs.

3.4. FTIR analysis of prepared Ag NPs and Au NPs

Fig. 5a&b display the FTIR spectra of synthesized Ag NPs and Au NPs. The spectra show characteristic peaks of many functional groups that are present in the prepared NPs. As pure metallic constituents will not constitute towards peaks obtained from FTIR analysis, the obtained peaks are from the biological moieties. The FTIR peaks obtained from Ag NPs and Au NPs and their corresponding characteristic functional groups are summarized in Table 2.

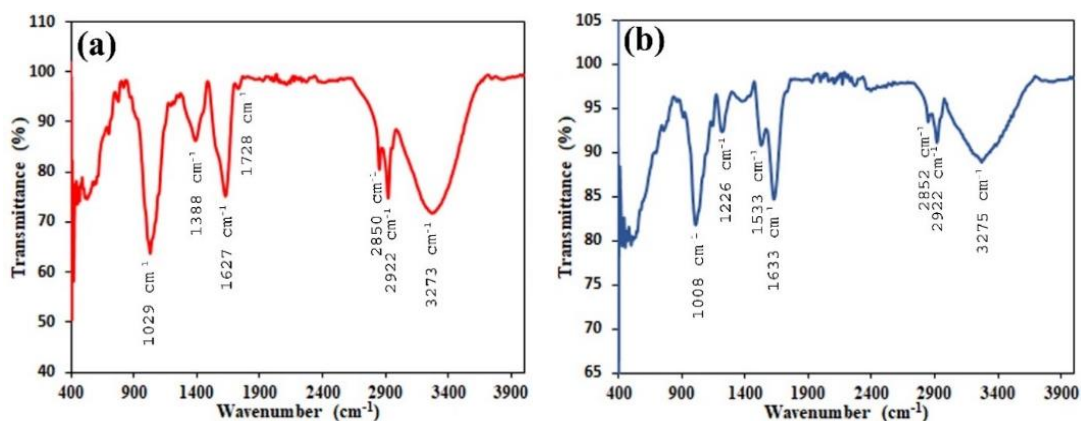


Fig. 5. FTIR spectra of (a) Ag NPs and (b) Au NPs

Table 2. FTIR peaks obtained from Ag NPs and Au NPs.

S. No.	Ag NPs		Au NPs	
	Wavenumber (cm ⁻¹)	Functional Group	Wavenumber (cm ⁻¹)	Functional Group
1	1029	C-O [17]	1008	C-O [17]
2	1388	C-H bending [17]	1226	C-N stretching amines [18]
3	1627	Chelated carbonyl group or -OH from carboxyl group [19]	1533	C=C aromatic [17]
4	1728	C-C stretching [18]	1633	Chelated carbonyl group or -OH from carboxyl group [19]
5	2850	C-H stretching [19]	2852	C-H stretching [19]
6	2922	C-H stretching [19]	2922	C-H stretching [19]
7	3273	O-H [17]	3275	O-H [17]

From the FTIR spectral report, it is clear that biological components are present along with Ag NPs and Au NPs acting as capping agent which improves the stability of the prepared particles. The biological components that act as antioxidants have the ability to donate electrons. Therefore, the surface metal ions over Ag NPs and Au NPs attract these antioxidants towards it and thus, acting as a capping agent.

3.5. Catalytic activity of Ag NPs and Au NPs through dye degradation studies

The catalytic behavior of the synthesized Ag NPs and Au NPs is followed by the UV-Vis spectrometer. The λ_{\max} for MB and CR is found at 664 nm and 498 nm, respectively. At first, the catalytic activity of combinations A and B are followed and the UV-Visible spectra recorded for a period of 20 min with 5 min intervals are shown in Fig. 6a&b. From the obtained spectra, it is clear that the presence of SB alone has negligible or no activity towards MB and CR. This result substantiates that while using SB as a reducing

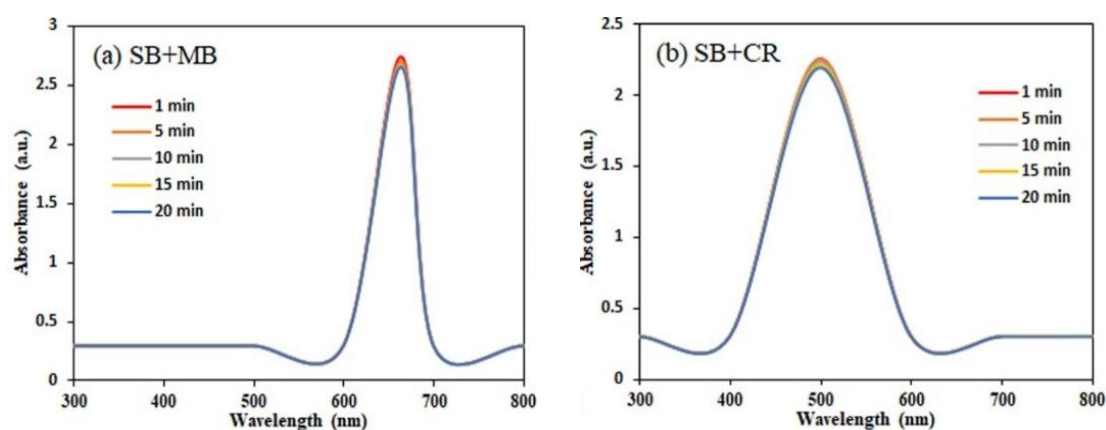


Fig. 6. UV-Visible spectra of (a) SB+MB and (b) SB+CR followed for 20 min.

agent, the activation energy for the reaction is high and doesn't readily reduce the selected dyes.

To elucidate whether there is any catalytic activity for the extract, experiments with respect to combination C and D are performed. The experiments are followed spectroscopically and the spectra are provided as Fig. 7a&b. From the Fig. , it is clear that the dyes are being reduced in the presence of extract. However, the rate of reaction is very less or not significant but higher compared to combination A and B.

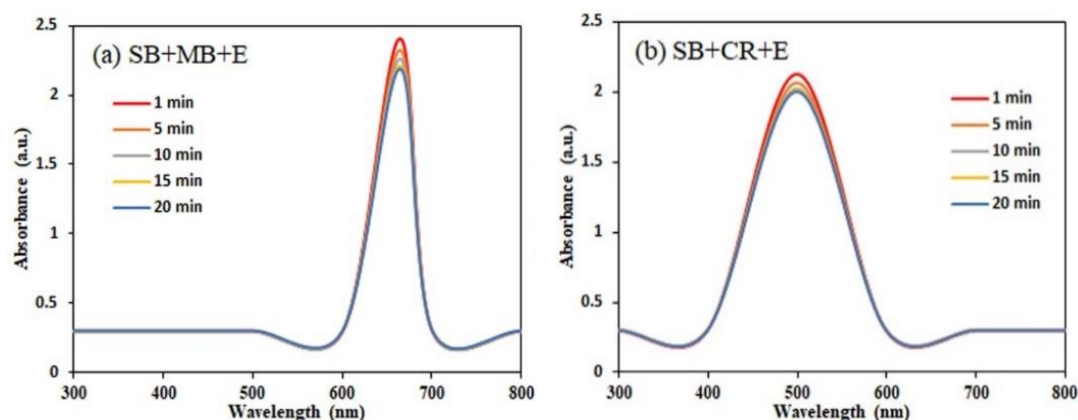


Fig. 7. UV-Visible spectra of (a) SB+MB+E and (b) SB+CR+E followed for 20 min

In contrast, in the presence of Ag NPs in the reaction mixture containing SB and dye (combination E and F), the dye degrades significantly. Fig. 8a&b show the UV-Visible spectra followed while degradation of MB and CR dyes in the presence of Ag NPs as a catalyst. From the figure, it is noted that 28% of MB and 25% of CR are being reduced in the presence of Ag NPs as catalysts substantiating the fact that Ag NPs readily reduce the activation energy for the reaction to occur. The change in the degradation rate for different dyes is due to their inherent chemical stability.

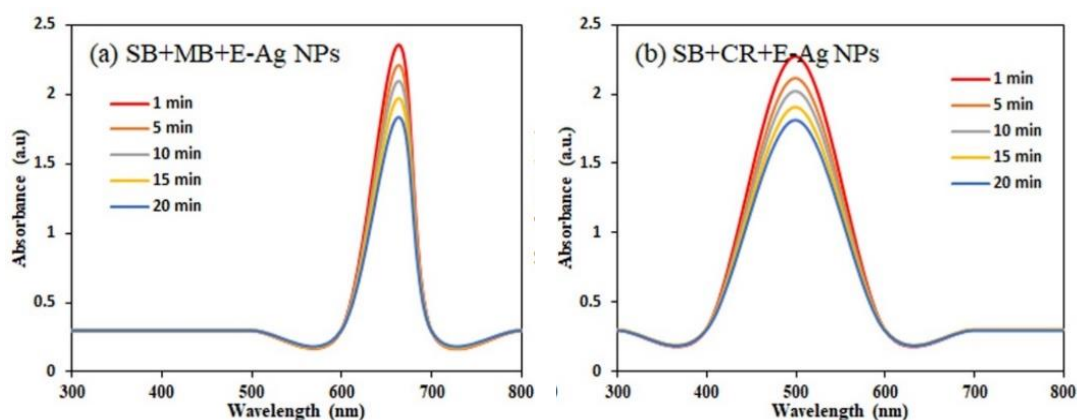


Fig. 8. UV-Visible spectra of (a) SB+MB+E-Ag NPs and (b) SB+CR+E-Ag NPs followed for 20 min

To further understand the activity of Au NPs as a catalytic agent, combination G and H are performed where the reactions are followed using UV-Visible spectroscopic data shown in Fig. 9a&b. From the obtained spectra, it is calculated that 66% of MB and 61% of CR are reduced owing to the catalytic behavior of Au NPs. Compared to Ag NPs, Au NPs displays better catalytic behavior due to the higher conductivity of Au moiety than Ag moiety. Here also, the CR dyes are found more stable than MB under catalytic reduction by Au NPs.

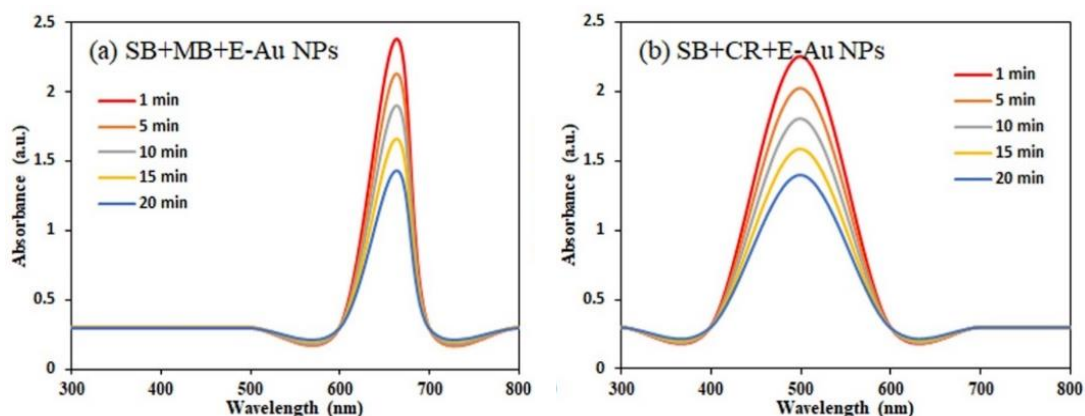


Fig. 9. UV-Visible spectra of (a) SB+MB+E-Ag NPs and (b) SB+CR+E-Ag NPs followed for 20 min

The steady-state catalytic reaction of Ag NPs and Au NPs could be described using the Langmuir–Hinshelwood relationship. At low levels, the degradation mechanism exhibits first-order kinetics that is expressed in simpler version as [11],

$$\frac{dA}{dt} = -K_A A$$

$$\ln\left(\frac{C_0}{C_t}\right) = K_A t$$

wherein K_A would be the degradation rate constant, A_0 denotes the dye's absorption at time 0, and A_t represents the dye's absorption at time t . A graph of $\ln(A_0/A_t)$ vs. degradation time for all samples is constructed to establish the rate constants of the degradation mechanism [Fig. 10]. Every plot is fitted linearly, where the rate constant, K_A is determined by the slope of the equation. The calculated rate constant results are listed in Table 3 using the first-order kinetic formula.

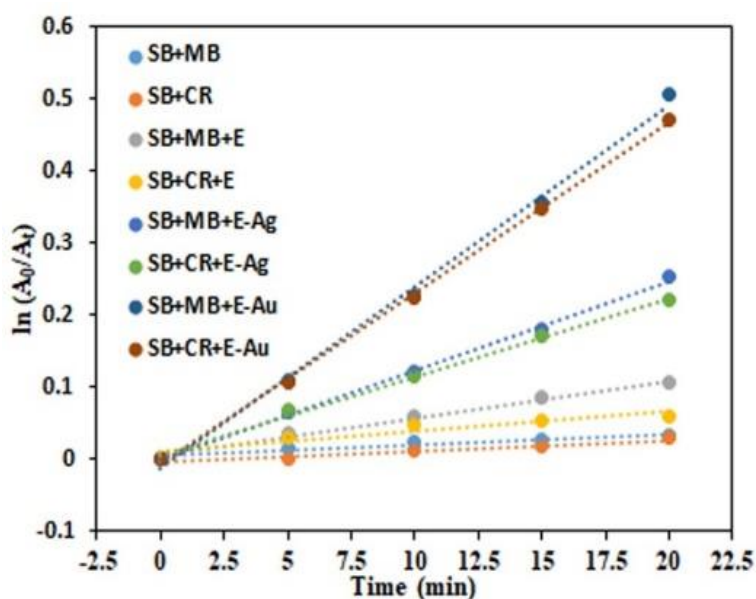


Fig. 10. The plot of $\ln(A_0/A_t)$ against time for the catalytic reduction of methylene blue dye and congo red dye in the existence of radish extract mediated silver nanoparticles

Table 3. Experimental results.

Sample composition	Linear equation	K_A (min^{-1})	Degradation efficiency (%)
SB+MB (A)	$y = 0.0016x + 0.0041$	0.0016	3
SB+CR (B)	$y = 0.0015x - 0.0028$	0.0015	3
SB+MB+E (C)	$y = 0.0052x + 0.0051$	0.0052	10
SB+CR+E (D)	$y = 0.0028x + 0.0097$	0.0028	6
SB+MB+E-Ag NPs (E)	$y = 0.0124x - 0.0008$	0.0124	28
SB+CR+E-Ag NPs (F)	$y = 0.0109x + 0.0058$	0.0109	25
SB+MB+E-Au NPs (G)	$y = 0.0252x - 0.0121$	0.0252	66
SB+CR+E-Au NPs (H)	$y = 0.0237x - 0.0072$	0.0237	61

The K_A numbers for experimental pairings A-H are 0.0016, 0.0015, 0.0052, 0.0028, 0.0124, 0.0109, 0.0252, and 0.0237, correspondingly, based on the slope of the formula. According to the K_A numbers, mixture G has a faster reaction rate than the other combinations, leading to extraordinary catalytic degradation of MB.

3.6. Mechanism of catalytic activity

As seen in Fig. 11, the dye degradation process could be described using the electron transport phenomenon. The electrons donating capacity of NaBH_4 and the electrons accepting ability of the pollutant molecules are closely related to the catalytic performance of Ag NPs or Au NPs. The molecules of NaBH_4 and the dye are first absorbed onto the surfaces of the NPs. NaBH_4 functions as a robust nucleophilic reagent after absorption, whereas the dye molecule works as an electrophilic reagent. In the reaction mixture, NPs operate as a relaying mechanism, assisting in the passage of the electron needed for dye degradation from NaBH_4 to the molecules [20]. The dye molecules are decomposed into small colorless compounds as CO_2 , H_2O , and others during the dye degradation mechanism. The results of this study show that by serving as a catalytic agent, Ag NPs or Au NPs may efficiently decompose single and multiple dyes from synthetic dye polluted wastewater.

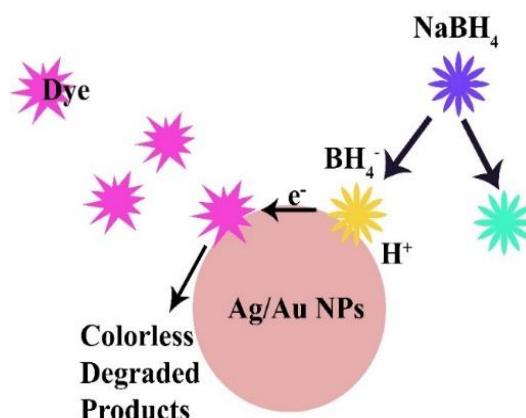


Fig. 11. Schematic representing the catalytic activity of Ag NPs or Au NPs

4. Conclusions

Radish peel waste extract has the phytochemicals like radish extract that reduce the Ag and Au metal salts to their respective NPs. The UV-visible spectral analysis display λ_{max} at 420 and 536 nm for Ag NPs and Au NPs, respectively. SEM analysis represents that the synthesized Ag NPs and Au NPs are spherical with size ranging from 35 nm to 55 nm for Ag NPs and from 40 nm to 50 nm for Au NPs. From the FTIR spectra, it is noticed that the synthesized Ag NPs and Au

NPs contain biological components that act as capping agents. Furthermore, the catalytic behavior of Ag NPs and Au NPs is estimated by degrading MB and CR in the presence of SB. From the obtained results, it is clear that the metallic NPs improve the rate of dye degradation where Au NPs displays better catalytic behavior than Ag NPs owing to its better conductivity. Thus, it is clear that the radish peel waste can be used for the synthesis of Ag NPs and Au NPs with catalytic behavior.

References

- [1] J. L. Gardea-Torresdey, E. Gomez, J. R. Peralta-Videa, J. G. Parsons, H. Troiani, M. Jose-Yacamán, *Langmuir* 19(4), 1357 (2003); <https://doi.org/10.1021/la020835i>
- [2] J. L. Gardea-Torresdey, J. G. Parsons, E. Gomez, J. Peralta-Videa, H.E. Troiani, P. Santiago, M. J. Yacamán, *Nano letters* 2(4), 397 (2002); <https://doi.org/10.1021/nl015673+>
- [3] A. Parveen, H. S. Mahdi, A. Azam, "Emerging Trends in Nanotechnology", 163 (2021); https://doi.org/10.1007/978-981-15-9904-0_6
- [4] U. Ullah, A. Rauf, E. El-Sharkawy, F. A. Khan, A. Khan, S. M. Bukhari, M. Thiruvengadam, *Bioprocess and Biosystems Engineering* 44(6), 1185 (2021); <https://doi.org/10.1007/s00449-020-02500-8>.
- [5] S. Jebril, A. Fdhila, C. Dridi, *Scientific Reports* 11(1), 1 (2021); <https://doi.org/10.1038/s41598-021-01609-4>
- [6] M. A. Solaiman, M. A. Ali, N. M. Abdel-Moein, E. A. Mahmoud, *Biocatalysis and Agricultural Biotechnology* 29, 101832 (2020); <https://doi.org/10.1016/j.bcab.2020.101832>
- [7] T. Ghosh, A. Chattopadhyay, A. C. Mandal, S. Pramanik, P. K. Kuir, *Chinese Journal of Physics* 68, 835 (2020); <https://doi.org/10.1016/j.cjph.2020.10.025>
- [8] M. Sivakumar, S. Surendar, M. Jayakumar, P. Seedeivi, P. Sivasankar, M. Ravikumar, M. Anbazhagan, T. Murugan, S. S. Siddiqui, S. Loganathan, *Journal of Cluster Science* 32(1), 167 (2021); <https://doi.org/10.1007/s10876-020-01775-x>
- [9] S. Mehta, S. Jha, H. Liang, *Renewable and Sustainable Energy Reviews* 134, 110345 (2020); <https://doi.org/10.1016/j.rser.2020.110345>
- [10] A. Azam, I. Khan, A. Mahmood, A. Hameed, *Journal of the Science of Food and Agriculture* 93(13), 3237 (2013); <https://doi.org/10.1002/jsfa.6165>
- [11] K. Jeyasubramanian, G. S. Hikku, M. Sivashakthi, *Materials Science in Semiconductor Processing* 51, 25 (2016); <https://doi.org/10.1016/j.mssp.2016.04.017>
- [12] G. Calabrese, S. Petralia, D. Franco, G. Nocito, C. Fabbi, L. Forte, S. Guglielmino, S. Squarzoni, F. Traina, S. Conoci, *Materials Science and Engineering: C* 118, 111394 (2021); <https://doi.org/10.1016/j.msec.2020.111394>
- [13] Q. J. Fadel, L. A. M. Al-Mashhedy, *Biotechnol Ind J* 13(1), 120 (2017).
- [14] S. Mickymaray, *Biomolecules* 9(11), 662 (2019); <https://doi.org/10.3390/biom9110662>
- [15] G. S. Hikku, R. K. Sharma, R. V. William, P. Thiruramanathan, S. Nagaveena, *Journal of Taibah University for Science* 11(4), 576 (2017); <https://doi.org/10.1016/j.jtusci.2016.02.002>
- [16] G. Geng, P. Chen, B. Guan, Y. Liu, C. Yang, N. Wang, M. Liu, *RSC advances* 7(82), 51838 (2017); <https://doi.org/10.1039/C7RA11188F>
- [17] M. Mousavi-Khattat, M. Keyhanfar, A. Razmjou, *Artificial cells, nanomedicine, and biotechnology* 46(sup3), S1022 (2018); <https://doi.org/10.1080/21691401.2018.1527346>
- [18] K. Jyoti, M. Baunthiyal, A. Singh, *Journal of Radiation Research and Applied Sciences* 9(3), 217 (2016); <https://doi.org/10.1016/j.jrras.2015.10.002>
- [19] T. P. Amaladhas, S. Sivagami, T. A. Devi, N. Ananthi, S. P. Velammal, *Advances in Natural Sciences: Nanoscience and Nanotechnology* 3(4), 045006 (2012); <https://doi.org/10.1088/2043-6262/3/4/045006>
- [20] D. Gola, N. Bhatt, M. Bajpai, A. Singh, A. Arya, N. Chauhan, S. K. Srivastava, P. K. Tyagi, Y. Agrawal, *Current Research in Green and Sustainable Chemistry* 4, 100132 (2021); <https://doi.org/10.1016/j.crgsc.2021.100132>